JMEPEG (2009) 18:1091–1101
DOI: 10.1007/s11665-008-9332-3

1059-9495/$19.00

Effects of Strain Rate and Temperature on Tensile Flow Behavior and Energy Absorption of Extruded Magnesium AM30 Alloy

S. Xu, W.R. Tyson, R. Bouchard, and V.Y. Gertsman

(Submitted April 30, 2008; in revised form November 14, 2008)

The effects of strain rate, temperature and texture on tensile flow stresses, and energy absorption of a magnesium extrusion AM30 alloy were experimentally determined over a range of strain rates (0.00075 and 9 s^{-1}) and temperatures (−143 and 100 °C). The extrusion has a texture such that the normals of the basal planes {0002} are approximately parallel to TD and the <11$\bar{2}$0> crystal orientation is parallel to ED (ED = extrusion direction, TD = long transverse direction, and ND = short transverse direction of the extrusion). Tensile strain along the ED was accompanied by only limited twinning before necking. The yield strengths of ED samples depend linearly on a rate parameter commonly used for thermally activated deformation. Thermal activation analysis indicates that the activation volume is essentially constant. Tensile deformation in the long transverse direction (TD) showed significant twinning during the initial 6-8% strain. The ductility is good, with average total elongations at 22 °C and a quasi-static rate of 12.3 and 19.1% in ED and TD directions, respectively. Nominal strain energy densities were evaluated up to 10% engineering strain and to fracture. The crashworthiness of the Mg extrusion, taking into account yield strength, ductility, and density, compares favorably to automotive Al alloys and high-strength steels.

Keywords AM30, constitutive equation, crashworthiness, effects of strain rate and temperature, magnesium alloy, nominal strain energy density, thermal analysis

1. Introduction

Intensive research and development (R&D) activities on magnesium alloys in automotive industry come from the promising advantages for economic, legislation, environment, and performance reasons. As automotive industry has actively engaged in the applications of Mg alloys, there is an increased use of Mg alloys in cars including large automotive structural applications such as front engine cradle (Ref 1) and cross-car beam (Ref 2). Crashworthiness-related mechanical properties of steels and Al alloys have been investigated extensively over the years because the automotive crash-critical components are made of various sheet and extrusion alloys of steel and aluminum. There is a desire to make crashworthy automotive components from Mg alloys in order to expand the use of lightweight Mg alloys in automobiles, which has focused attention for example on magnesium front-end body structure design and manufacturing (Ref 3). However, information on crashworthiness of Mg alloys is less available than that of steel and Al alloys, especially for new Mg alloys with improved chemistry and/or novel processing. Wrought magnesium alloys generally have better strength and ductility than those of cast magnesium alloys. Extrusions of alloy AM30, for example, are of interest for structural components, and are being evaluated in an on-going international Magnesium Front-End Research and Development (MFERD) project (Ref 3). AM30 is a newly developed Mg alloy having improved extrudability and formability (Ref 4, 5), and detailed examinations on deformation behavior and mechanisms have been performed on extruded tubes (e.g., Ref 6, 7). For design and simulation of crashworthiness, mechanical properties such as flow stress are required over a range of strain rates, temperatures, orientations and loading paths. These data are required for development of reliable material models (constitutive equations), increasingly needed as input for computer-aided engineering (CAE) modeling.

In the present work, tensile flow properties of a large extrusion of AM30 alloy were experimentally investigated over a range of strain rates and temperatures. The strain rates varied over five orders of magnitude. The temperature range was between −143 °C (~0.14 T_m, where T_m is the melting temperature in Kelvin) and 100 °C (~0.40 T_m) and covers the range of interest for normal use of automotive alloys, i.e., −50 to 100 °C. Anisotropy was studied by taking samples along the extrusion direction (ED) and the long transverse direction (TD). Absorbed energies in tensile tests were also calculated, which are especially of interest for crashworthiness performance. Tensile flow properties and absorbed energies are reported in detail in graphic and tabulated format. Investigation of compressive flow behavior of the extrusion is under way and will be reported in the future.

S. Xu, W.R. Tyson, R. Bouchard, and **V.Y. Gertsman**, CANMET-Materials Technology Laboratory, Natural Resources Canada, 568 Booth St., Ottawa, Ontario, Canada K1A 0G1. Contact e-mail: sxu@nrcan.gc.ca.

2. Material and Experimental Procedure

Large solid extrusions of AM30 alloy were extruded at Timminco, Aurora, Colorado, USA. The alloys were extruded at temperatures between 360 and 382 °C, at an extrusion ratio of approximately 6, and air-quenched. The cross-section dimensions of the thick part of the extrusions were 76 mm (in the long TD) × 22 mm (in the short ND). Figure 1 shows the Mg extrusion and orientation designation. Samples were taken from the thick section. The macrograph of an etched cross section taken normal to ED is shown in Fig. 2; grains were uniform and equi-axed in most of the extrusion except for a very limited coarse-grain region near the surface that was not used in machining of samples. Chemical compositions were obtained using spectrographic analysis, averaged over six spots in the near surface regions and are given in Table 1.

Dog-bone type tensile specimens with a gage length of 25.4 mm and diameter of 6.34 mm were machined so that their axes were either in ED or TD directions. Tensile samples were cut out of the center region of the extrusions. Tests were carried out over a range of strain rates (0.00075 and 9 s^{-1}) and temperatures (−143 and 100 °C) using a servohydraulic testing machine and an environmental chamber. The strain rates were controlled and estimated by cross-head rates and the tensile strains were monitored using an extensometer. The samples were held for about 15 min. after the samples reached test temperature before testing.

Micrographs were taken near the central axis of fractured tensile samples sectioned about 15 mm from the fracture surfaces and etched using an acetic-picral etchant (5 mL acetic acid, 6 g picric acid, 10 mL H_2O, and 100 mL ethanol (95%)).

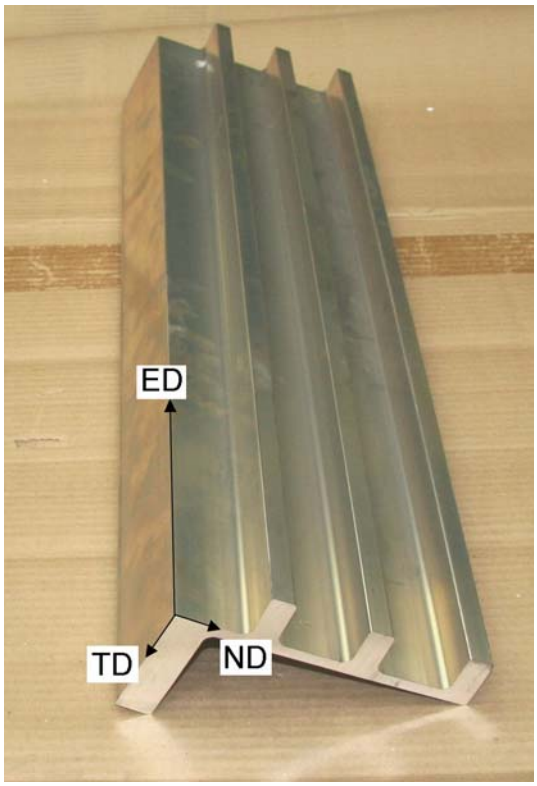

Fig. 1 Photo of Mg extrusion and orientation designation (samples were taken from the thick section)

Transmission electron microscopy (TEM) samples were prepared from the regions within the gage length, half-way between the fracture surface and the end of the reduced section. The TEM samples were 3-mm diameter disks ground to approximately 70-100 μm thick. The disks were electrolytically polished using an electrolyte (5% $HClO_4$, 15% ethylene glycol and 80% Methanol) at 16 Volts, 10 mA, and −35 °C for approximately 2.5 min.

3. Results

3.1 Microstructure and Texture of As-received Extrusion

Optical micrographs of as-received AM30 extrusion sectioned normal to TD, ED, and ND directions are shown in Fig. 3. The grains in all three sections of the AM30 extrusion were equi-axed, and the mean intercept grain size measured in the section normal to ED was approximately 32 μm. Twins may be observed in all sections (Fig. 3).

Texture was measured by X-ray diffraction in the central parts of the extrusion. The pole figures are shown in Fig. 4. The texture is such that the normals of basal planes {0002} are essentially aligned parallel to TD and the $<11\bar{2}0>$ axis is parallel to the ED direction. The texture of Mg extruded at relatively low temperatures (300-500 °C) is typically of {0001} $<01\bar{1}0>$ type (Ref 8), i.e., the normal of {0001} parallel to ND and $<01\bar{1}0>$ parallel to ED, in contrast to that in the as-received AM30 extrusion. The prism $\{01\bar{1}0\}$ planes are parallel to the TD direction. The texture in the AM30 extrusion results from processing, which involves both deformation (extrusion) and recrystallization. The existence of texture in the extrusions is the main reason for mechanical anisotropy along different orientations as observed in this investigation.

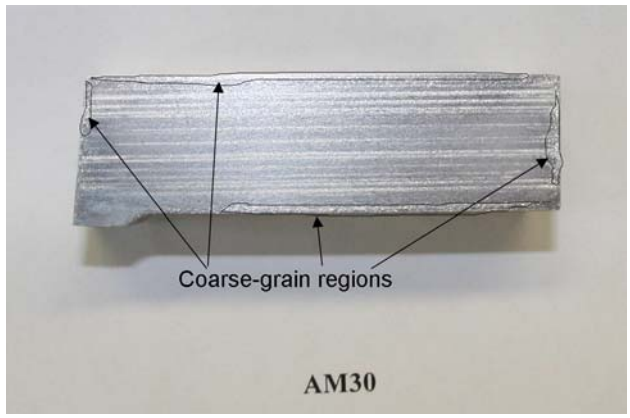

Fig. 2 Etched cross section showing only limited coarse-grain region near surface

Table 1 Chemical composition of AM30 extrusion (wt.%)

Extrusion	Mg	Al	Mn	Si	Zn	Cu	Fe	Ni
AM30	Balance	3.0	0.38	0.013	<0.05	<0.005	0.003	0.0005

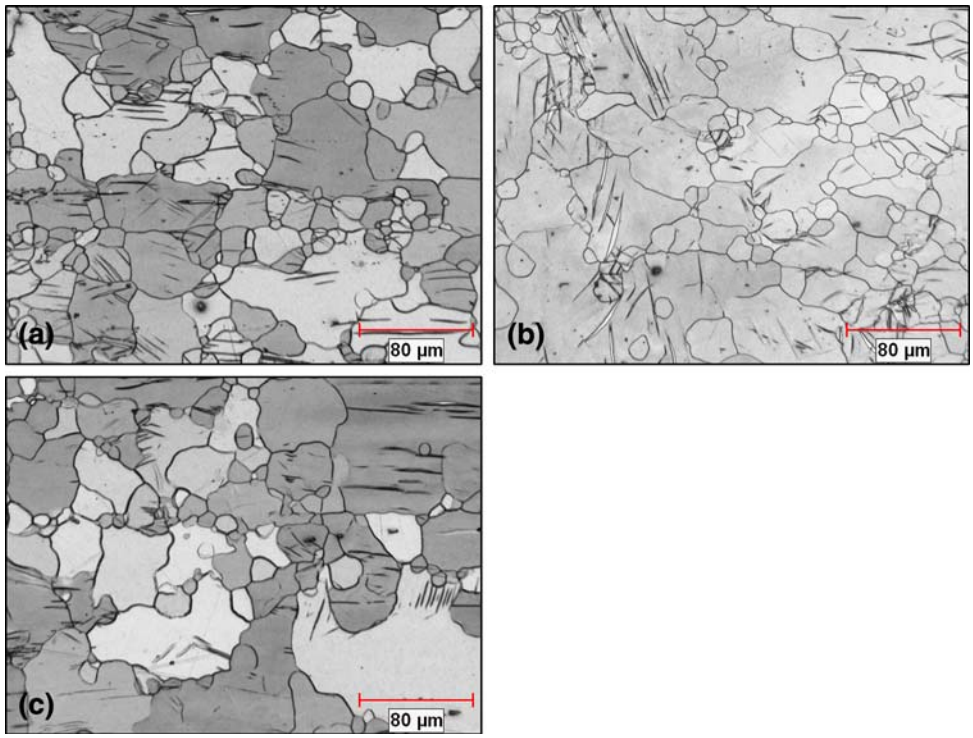

Fig. 3 Optical micrographs of AM30 extrusion. (a) Section with normal parallel to TD (b) Section with normal parallel to ED, and (c) Section with normal parallel to ND

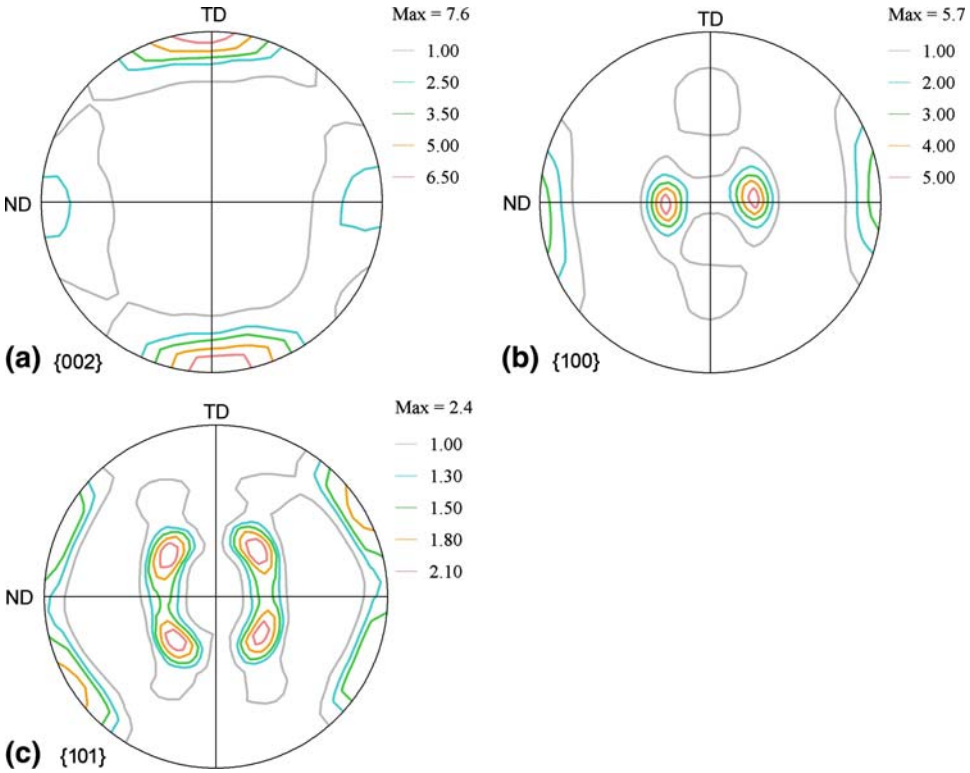

Fig. 4 Pole figures of AM30 extrusion (Note: $\{002\} = \{0002\}$, $\{100\} = \{10\bar{1}0\}$, and $\{101\} = \{10\bar{1}1\}$). (a) {002}, (b) {100}, and (c) {101}

3.2 Microstructure of Deformed Samples

Metallographic examinations on cross-sections of tensile tested ED and TD samples away from fracture surfaces (i.e., at strains approximately corresponding to ultimate tensile strength, UTS) showed that in the ED samples the twin density was approximately the same as in the as-received condition (Fig. 5a).

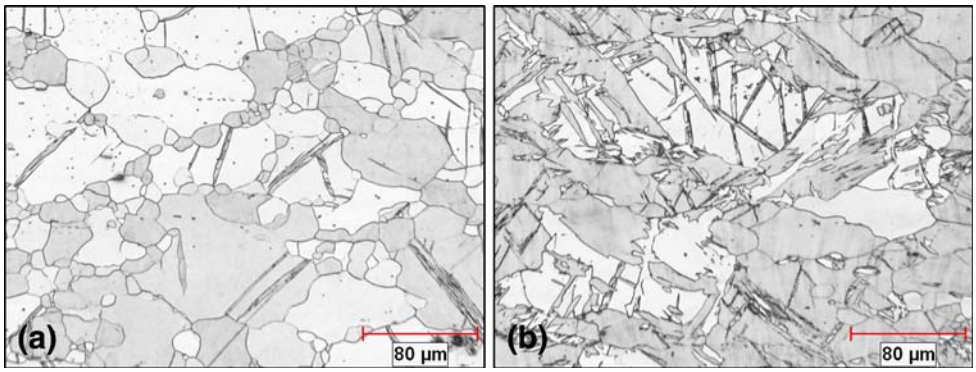

Fig. 5 Optical micrographs of tensile samples after deformation at 0.00075 s^{-1} and 100 °C. (a) ED sample, (b) TD sample

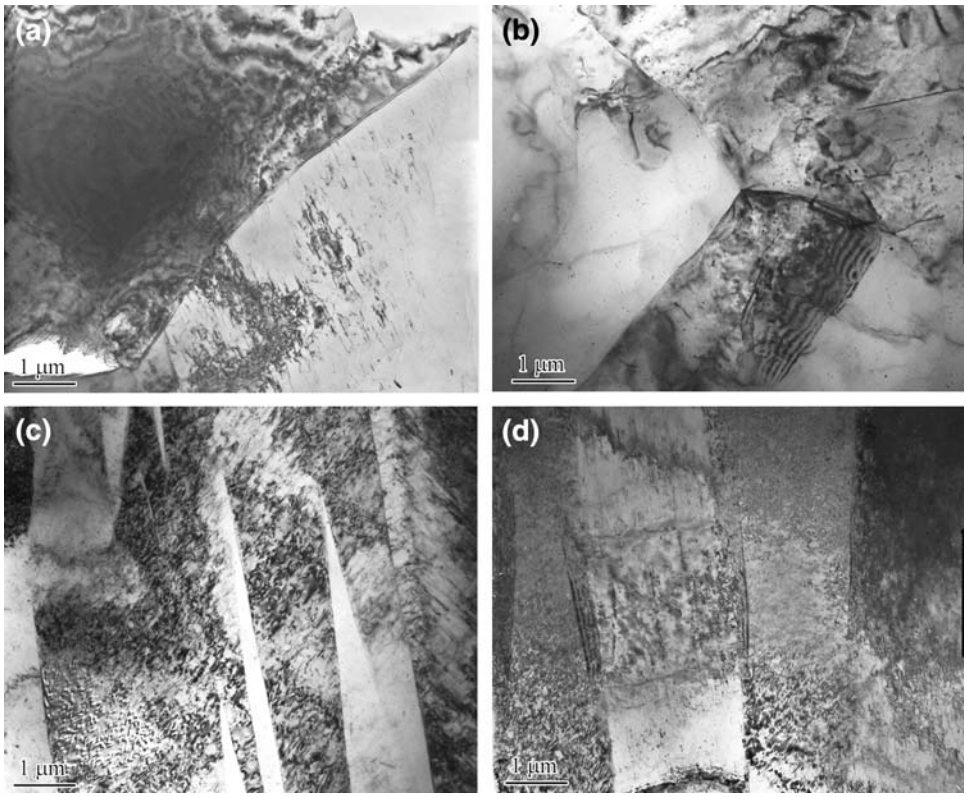

Fig. 6 TEM micrographs of deformed AM30 samples: (a) ED, 0.00075 s^{-1}, −110 °C, (b) ED, 0.00075 s^{-1}, 100 °C, (c) TD, 0.00075 s^{-1}, −50 °C, and (d) TD, 0.00075 s^{-1}, 100 °C

At the same time, significant twinning was observed in the TD samples (Fig. 5b).

Microstructures of the samples tensile tested to fracture at the same strain rate, but different temperatures were examined in TEM. Representative micrographs are shown in Fig. 6. The TEM observations can be summarized as follows. There is little difference in the dislocation and twin densities in the samples tested in the same orientation at different temperatures. However, the tensile sample orientation has a crucial effect in the deformation microstructure: the densities of dislocations and twins are higher in the TD samples than in the ED samples. The TEM observations regarding twinning are in accord with the optical metallography results (see above).

3.3 Tensile Flow Behavior

The tensile stress-strain curves of the extrusion showed excellent repeatability. Tensile stress-strain curves at room temperature and quasi-static rate (usually between 10^{-5} s^{-1} and 10^{-3} s^{-1}) are shown in Fig. 7 for samples machined in both ED and TD directions. Tensile stress-strain curves along ED can be roughly approximated by a power-law relation while those along TD exhibited a sigmoidal shape. This is consistent with the observations (see above) that tensile strain along ED involved limited twinning while strain along TD showed significant twinning during the first 6-8% strain as will be discussed later. Tensile total elongations of ED samples are less

than those of TD samples. This indicates the beneficial twinning contribution to the plasticity of the TD tensile samples. The ductility of the Mg alloy is good with average total elongations at 22 °C and a quasi-static rate of 12.3 and 19.1% for ED and TD directions, respectively. Tensile properties (yield strength (YS), ultimate tensile strength (UTS), total elongation and reduction of area (R.A.)) at different temperatures and strain rates are summarized in Table 2 and 3 for ED and TD samples, respectively. Strain-hardening exponents (n) for ED samples are also included in Table 2; n values were determined according to ASTM E 646 using data for curve-fitting between the yield to maximum loads.

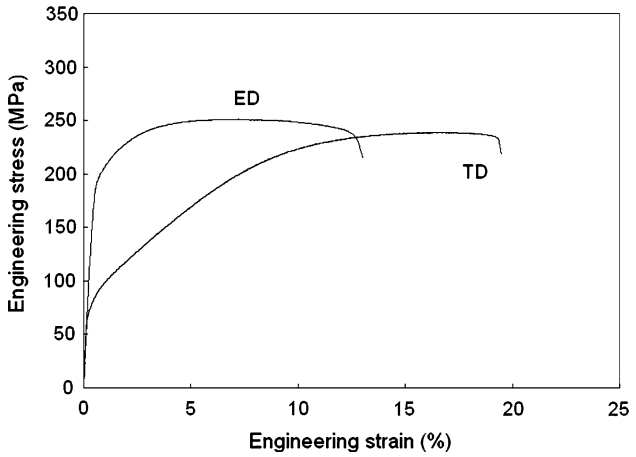

Fig. 7 Effect of orientation on tensile stress-strain curves at 0.00075 s^{-1} and 22 °C

To provide data for crashworthiness simulations and constitutive analyses, tensile tests were performed over a range of strain rates (0.00075-9 s^{-1}) and temperatures (−143 to 100 °C). Typical stress-strain curves showing the effects of strain rate and temperature are shown in Fig. 8 and 9, respectively. With increase of strain rate and decrease of temperature, flow strength generally increases while total elongation decreases in ED samples at temperatures above 23 °C and in TD samples. Tensile tests performed along ED exhibited a significant effect of strain rate and temperature. The effects of strain rate and temperature on TD samples are smaller than the ED samples at the initial stage of deformation; this depends on the extent of twinning activity, i.e., the more significant the twinning activity, the less the effects of strain rate and temperature as will be discussed later. Effects of temperature on YS in ED and TD are shown in Fig. 10. For ED samples, yield strengths rose 86% for a decrease of temperature from 100 to −143 °C at 0.00075 s^{-1}. Similarly, yield strengths at 22 °C increased 28% for a strain rate increase from 0.00075 to 9 s^{-1}. Effects of strain rate and temperature on UTS and total elongation in ED samples, as discussed above, are summarized in Fig. 11 and 12.

3.4 Nominal Strain Energy Density

In general, structural crashworthiness refers to the load-carrying capacity or energy absorption capacity. For crashworthiness performance, nominal strain energy density, defined as absorbed energy divided by the initial volume, up to 10% engineering strain is conventionally considered as a relevant parameter for steels (Ref 9-11). Nominal strain energy density up to fracture during tensile tests can also be used as a qualitative indication of mechanical performance of materials

Table 2 Tensile properties (ED) of extruded AM30 at different temperatures and strain rates

T, °C	Strain rate, s^{-1}	YS, MPa	UTS, MPa	Total elongation, %	R.A., %	n
100	0.00075	150 (148, 152)*	207 (203, 211)	28.8 (26.6, 31.0)	39.1 (36.6, 41.5)	0.132 (0.126, 0.138)
50		179 (168, 189)	237 (234, 240)	17.3 (17.4, 17.1)	28.4 (27.7, 29.0)	0.127 (0.125, 0.129)
22		196 (195, 196, 196)	250 (249, 251, 250)	12.3 (12.0, 12.7, 12.3)	20.8 (18.0, 23.4, 21.1)	0.130 (0.130, 0.129, 0.130)
−20		221 (216, 227)	275 (275, 275)	9.9 (10.0, 9.8)	15.9 (16.0, 15.7)	0.130 (0.136, 0.124)
−50		241 (241, 240)	293 (297, 290)	10.2 (11.0, 9.3)	12.2 (13.7, 10.7)	0.123 (0.130, 0.116)
−80		254 (248, 260)	320 (318, 321)	10.1 (10.4, 9.8)	13.7 (13.4, 14.0)	0.121 (0.129, 0.112)
−110		274 (282, 266)	349 (354, 344)	8.7 (10.0, 7.4)	10.3 (11.3, 9.2)	0.145 (0.141, 0.148)
−143		279 (284, 273)	371 (372, 370)	7.8 (7.9, 7.7)	9.5 (9.2, 9.8)	0.174 (0.176, 0.172)
100	0.02	168 (158, 178)	220 (219, 221)	20.6 (20.9, 20.3)	32.1 (30.1, 34.0)	0.105 (0.101, 0.109)
50		190 (186, 193)	239 (239, 238)	12.6 (13.1, 12.0)	20.1 (22.5, 17.7)	0.107 (0.096, 0.117)
22		205 (187, 224)	260 (254, 265)	11.6 (11.8, 11.3)	19.5 (18.9, 20.0)	0.116 (0.115, 0.117)
−50		247 (249, 245)	298 (296, 299)	9.2 (9.0, 9.4)	12.8 (13.4, 12.2)	0.113 (0.106, 0.119)
−80		263 (264, 261)	328 (329, 326)	9.5 (10.2, 8.7)	11.2 (11.6, 10.7)	0.134 (0.133, 0.134)
−143		277 (284, 269)	380 (382, 379)	7.0 (6.9, 7.0)	9.7 (10.4, 8.9)	0.180 (0.176, 0.184)
100	1	213 (223, 204)	234 (240, 229)	13.8 (14.3, 13.3)	31.4 (35.3, 27.5)	0.084 (0.084, 0.083)
50		207 (197, 217)	242 (240, 243)	11.2 (11.5, 10.8)	17.6 (18.0, 17.1)	0.078 (0.073, 0.083)
22		230 (227, 233)	259 (255, 263)	10.9 (10.4, 11.3)	13.0 (13.4, 12.5)	0.085 (0.078, 0.092)
−50		260 (261, 258)	322 (322, 323)	9.6 (10.2, 8.9)	13.0 (13.4, 12.5)	0.130 (0.122, 0.137)
−80		270 (252, 288)	354 (349, 360)	9.2 (8.8, 9.6)	11.0 (10.7, 11.3)	0.147 (0.154, 0.139)
−143		291 (298, 284)	405 (409, 402)	8.0 (7.8, 8.1)	9.4 (8.9, 9.8)	0.182 (0.177, 0.186)
100	9	231	240	13.7	52.2	0.025
22		251 (256, 246)	277 (279, 275)	13.7 (14.0, 13.4)	30 (32, 28)	0.087 (0.091, 0.083)
−50		269	343	11.2	16.3	0.142
−143		303	409	6.7	8.6	0.203

* Figures in brackets are individual values of duplicate tests

Table 3 Tensile properties (TD) of extruded AM30 at different temperatures and strain rates

T, °C	Strain rate, s^{-1}	YS, MPa	UTS, MPa	Total elongation, %	R.A., %
100	0.00075	72 (71, 73)*	191 (191, 192)	39.7 (37.3, 42.0)	46.2 (45.0, 47.4)
50		74 (73, 76)	223 (223, 223)	24.7 (25.0, 24.4)	26.8 (27.5, 26.1)
22		76 (76, 76, 77)	239 (239, 239, 239)	19.1 (19.3, 18.9, 19.1)	20.5 (22.5, 19.7, 19.2)
−20		80 (80, 80)	266 (265, 267)	15.8 (15.6, 16.0)	15.9 (15.7, 16.0)
−50		87 (89, 84)	284 (284, 284)	14.2 (14.1, 14.3)	13.7 (13.4, 14.0)
−143		118	313	5.2	5.6
100	0.02	72	204	31.7	36.6
50		77 (78, 76)	229 (230, 229)	18.7 (18.4, 19.0)	17.5 (16.3, 18.6)
22		76 (77, 75)	242 (242, 242)	17.2 (16.5, 17.8)	15.9 (15.4, 16.3)
−50		85 (84, 89, 84)	287 (288, 281, 291)	11.6 (12.0, 10.1, 12.8)	11.9 (···**, 11.9)
−143		88	307	7.2	
100	1	80 (80, 79)	217 (217, 216)	20.4 (20.0, 20.7)	22.0 (21.4, 22.5)
50		77 (76, 77)	237 (237, 237)	16.4 (16.4, 16.4)	16.9 (17.5, 16.3)
22		88 (87, 90)	256 (256, 255)	15.3 (15.1, 15.4)	16.6 (16.3, 16.9)
−50		106 (115, 123, 81)	298 (300, 294, 300)	8.9 (10.1, 5.9, 10.8)	···
−143		112	310	4.7	···
100	9	77	217	17.7	21.9
22		86 (82, 91)	269 (269, 268)	17.0 (16.3, 17.0)	15.9 (15.4, 16.3)
−50		113	299	7.1	8.3

* Figures in brackets are individual values of duplicate tests
** Samples were fractured outside the gage length and R.A. values were not determined

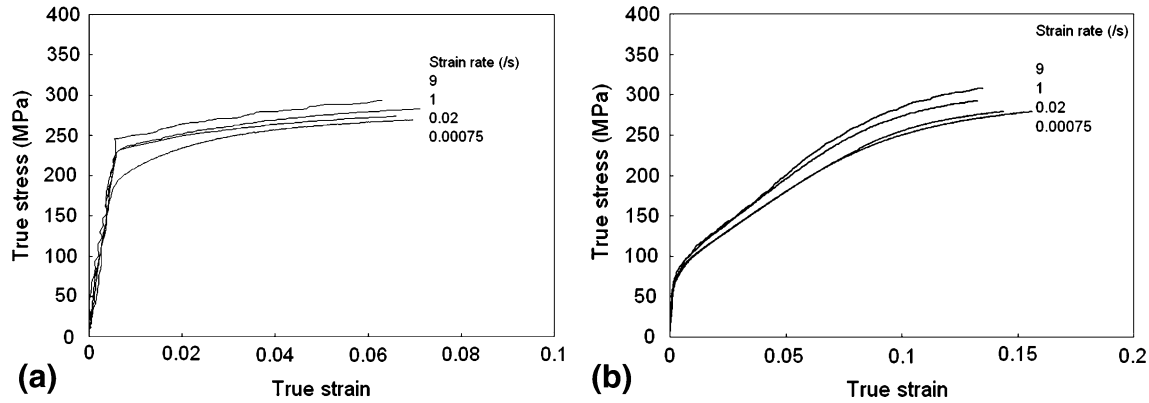

Fig. 8 Effect of strain rate on tensile flow curves in the indicated direction at 22 °C. (a) ED, (b) TD

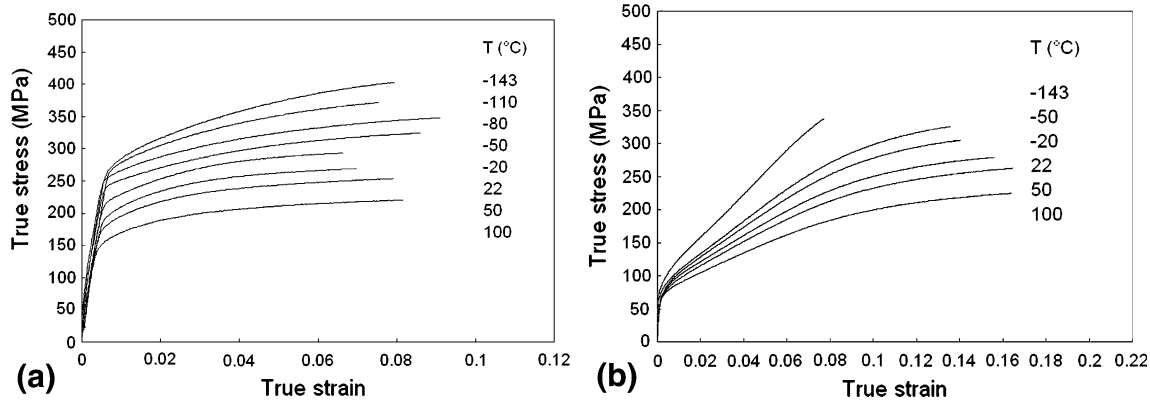

Fig. 9 Effect of temperature on tensile true stress-strain curves in the indicated direction at 0.00075 s^{-1}. (a) ED, (b) TD

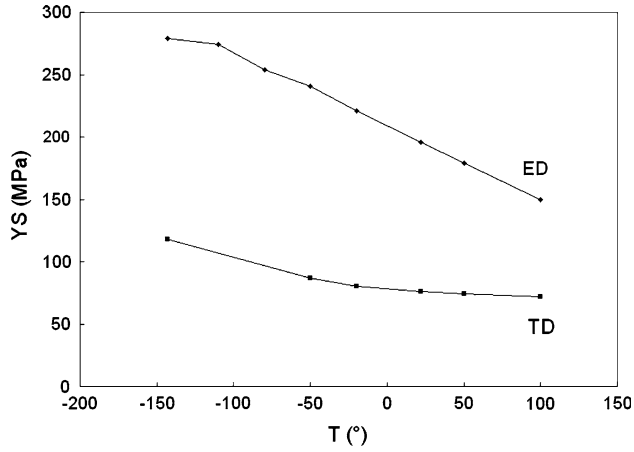

Fig. 10 Effect of temperature on YS at 0.00075 s^{-1}

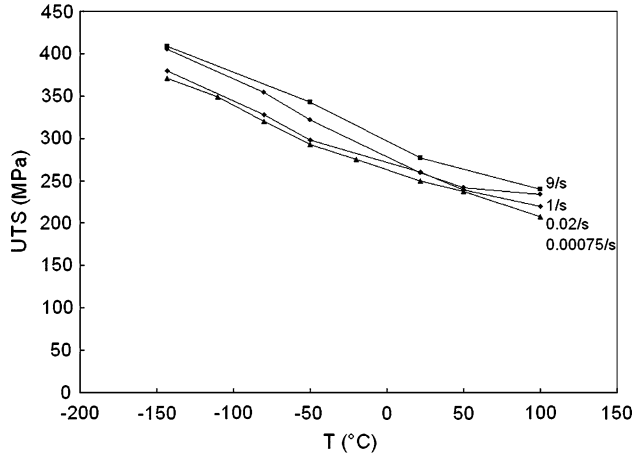

Fig. 11 Effects of strain rate and temperature on UTS in ED direction

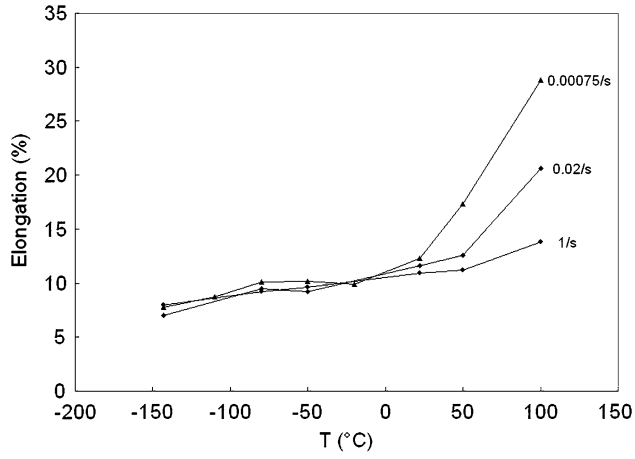

Fig. 12 Effects of strain rate and temperature on total elongation in ED direction

(e.g., Ref 12). In this work, both nominal strain energy densities up to 10% engineering strain ($W_{0.1}$) and to fracture (W_f) were calculated from engineering stress (s) versus engineering strain (e) curves according to the following relations,

Table 4 Nominal strain energy density of extruded AM30 under tension at different temperatures and strain rates

		$W_{0.1}$, MJ/m^3		W_f, MJ/m^3	
T, °C	Strain rate, s^{-1}	ED	TD	ED	TD
100	0.00075	19.3	13.6	51.4	64.7
50		22.2	15.4	50.5	48.8
22		23.7	16.4	34.0	39.0
−20		25.9	17.9	27.0	37.8
−50		28.0	19.1	35.4	34.2
−80		29.8		32.3	
−110		N/A*		25.1	
−143		N/A	N/A	27.7	17.2
100	0.02	21.1	14.4	46.4	57.2
50		23.1	16.2	30.7	36.0
22		25.4	16.4	34.5	36.2
−50		N/A	19.5	28.9	27.2
−80		30.8		33.2	
−143		N/A	N/A	26.0	16.9
100	1	22.1	15.8	32.6	39.3
50		23.4	16.9	30.3	33.7
22		25.4	17.9	31.2	35.5
−50		30.4	19.5	33.1	27.2
−80		33.7		35.1	
−143		N/A	N/A	31.7	16.0
100	9	22.8	15.5	30.4	33.1
22		27.5	18.2	36.9	37.1
−50		31.5	N/A	36.3	18.5

* N/A: not applicable (samples were broken before 10% strain)

$$W_{0.1} = \int_0^{0.1} \text{sde} \qquad \text{(Eq 1)}$$

and

$$W_f = \int_0^{e_f} \text{sde} \qquad \text{(Eq 2)}$$

where e_f is the engineering strain at fracture in a tensile test. Since the repeatability of tensile test results was excellent, the nominal strain energy densities were calculated from a representative test for each alloy/orientation/strain rate/temperature condition and are given in Table 4. Generally, increase of strain rate and decrease of temperature result in an increase of $W_{0.1}$ but a decrease of W_f. $W_{0.1}$ is mainly controlled by YS while W_f is strongly affected by total elongation. Examples showing the effects of temperature are shown in Fig. 13.

W_f may also be used to calculate other general mechanical performance evaluation parameters such as the so-called specific tensile performance parameter (Ref 12) which takes density into account for comparing materials. The specific tensile performance is defined as (Ref 12)

$$Q_{os} = \frac{YS}{\rho} + \alpha \frac{W_f}{\rho} \qquad \text{(Eq 3)}$$

where YS/ρ is the specific yield strength, W_f accounts for tensile ductility and α is a dimensionless coefficient selected to balance the contribution of strength and ductility (α = 10 for Mg alloys). Comparisons of W_f and the specific tensile

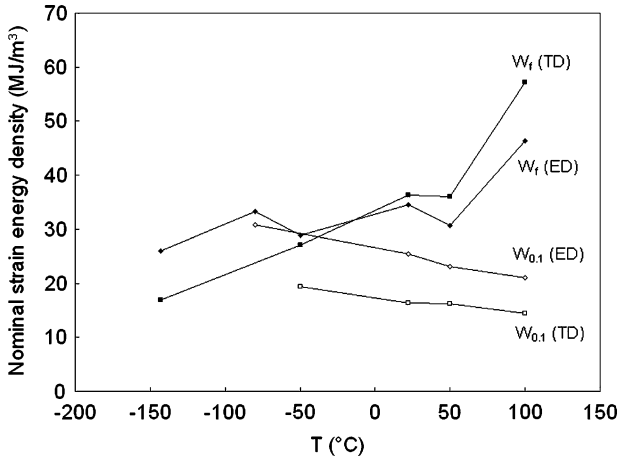

Fig. 13 Effects of temperature and orientation on nominal strain energy density of AM30 at 0.02 s^{-1}

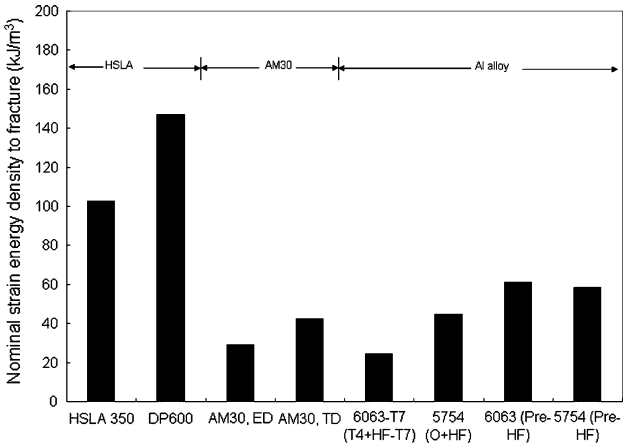

Fig. 14 Nominal strain energy density to failure of typical HSLA steels and Al alloys compared with AM30 extrusion

performance parameters of alloys of interest—Al alloys (AA6063 and AA5754), HSLA steels (HSLA350 and DP600) and the AM30 Mg extrusion—are shown in Fig. 14 and 15 for room temperature and quasi-static strain rate. The data for Al alloys and steels were taken from (Ref 13, 14) where detailed compositions and treatments are reported. The nominal strain energy density up to fracture (W_f) of steels and Al alloys were estimated from UTS and engineering total elongation at fracture (e_f) using the following equation (Ref 12)

$$W_f = \frac{UTS \cdot (1 + e_f) \cdot \ln(1 + e_f)}{\ln(1 + e_f) + 1}. \quad \text{(Eq 4)}$$

W_f of typical steels are higher than those of Al alloys and AM30 extrusion owing to their higher YS while low density and good ductility of Mg extrusions contribute to the high-specific tensile performance of the Mg alloy.

It should be pointed out that the nominal strain energy density is defined as the area under a nominal stress-strain curve up to fracture, and so varies with gage length. The comparison with data, especially W_f, obtained from different specimen geometries should be made with caution. If uniform strain is larger than 10%, $W_{0.1}$ would be less dependent on specimen geometry.

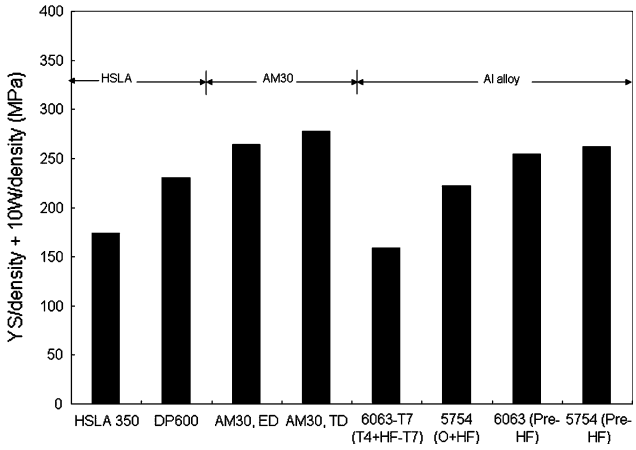

Fig. 15 Specific tensile performance of typical HSLA steels and Al alloys compared with AM30 extrusion

4. Discussion

4.1 Effect of Orientation and Deformation Mechanisms

Early work on deformation mechanisms of Mg alloys has been summarized by Roberts (Ref 15). Recently, deformation mechanisms of polycrystalline Mg and its alloys have been studied experimentally (electron backscatter diffraction, EBSD, and neutron diffraction) and through modeling (e.g., the viscoplastic self-consistent model) (Ref 6, 7, 16-22). It is well known that more slip systems, e.g., prismatic and pyramidal, must be operative in addition to basal slip for deformation of polycrystalline Mg. Twinning such as tension twinning $\{10\bar{1}2\}<10\bar{1}\bar{1}>$, contraction twinning $\{10\bar{1}1\}<10\bar{1}\bar{2}>$, and double twinning can significantly contribute to total strain, especially at small strains (in this work, up to 6 and 8%).

For Mg and its alloys, which have HCP crystal structure, the principal twinning is of the $\{10\bar{1}2\}<10\bar{1}\bar{1}>$ type and occurs when the basal plane is compressed or the prism plane is stretched (Ref 23). The texture of the AM30 extrusion is such that the basal planes are approximately perpendicular to TD. Therefore, twinning would not be active during tensile deformation of ED samples but would occur during tensile deformation of TD samples. This is reflected in the typical shapes of tensile stress-strain curves for ED and TD samples.

Based on the observations and information in open literature, the deformation mechanisms of the AM30 alloys under tension are assumed to be mainly dislocation slip for ED samples and twinning plus slip for TD samples. The volume fraction of twins increases with strain according to an approximately linear relationship in the initial 5-8% strain (Ref 24, 25) or a sigmoidal relationship over a large strain range (Ref 7). As the twinning contribution becomes exhausted, the work-hardening rate increases rapidly for TD samples; they also show a larger uniform and total elongation than those of the ED samples. This explains why strain energy densities up to 10% engineering strain ($W_{0.1}$) are higher for ED than for TD samples, while W_f values of TD samples at temperatures ≥ 22 °C are higher than those of ED samples (Fig. 13 and 14).

4.2 Effect of Strain Rate and Temperature

For ED samples, the effects of strain rate and temperature on tensile flow stress are significant. Stress-strain curves are

approximately parallel upon changes of strain rate and temperature (Fig. 8a and 9a). This is considered to be owing to thermally activated dislocation slip. For TD samples, the effects of strain rate and temperature are small initially and become more pronounced as the strain increases (Fig. 8b and 9b). This is because twining is stress controlled, i.e., activated by stress rather than temperature (athermal) (Ref 23), and deformation twinning dominates initially. The mechanical test results are consistent with TEM observations that there is little difference between the deformed microstructure of the samples at high and low temperatures but there is a large difference between the ED and TD samples (see Fig. 5). The TD samples showed more twins and dislocations.

The maximum possible adiabatic temperature rise, estimated using the parameters of stress (UTS) = 430 MPa, uniform elongation = 8%, specific heat = 1.02 J/(g·K) and density = 1.74 g/cm^3, is estimated to be about maximum 20^o K up to the UTS. Therefore, adiabatic heating is not significant for the tensile tests up to UTS in the Mg alloy samples, i.e., the true stress-strain curves determined in this work.

4.3 Constitutive Equation and Thermal Activation Analysis

Constitutive equations, i.e., flow stress as a function of strain, strain rate, and temperature, are of interest for Mg extrusions in crashworthiness analysis. For the extruded Mg alloys, the constitutive behavior is complicated by the contribution of twinning such as in TD samples. Flow stress up to large strain is relevant to crashworthiness simulation and design. The Johnson-Cook equation (Ref 26) is widely used as an empirical material model for crashworthiness modeling but extrapolation beyond the test data range is unreliable. The data reported in this work forms a database for constitutive analysis, presented below.

The effects of strain rate and temperature on flow stress is associated with the thermally activated deformation process in metals. (Note that the following analyses apply to true stress (σ) and strain (ε).) If the rate of plastic deformation is controlled by a single thermally activated dislocation mechanism, the thermal activation process could be described by an Arrhenius type equation (Ref 27, 28)

$$\dot{\varepsilon} = \upsilon \exp - \left(\frac{\Delta H}{kT}\right) \quad \text{(Eq 5)}$$

where υ is a frequency factor that includes the number units involved in the deformation, the frequency of vibration, and an entropy term; and ΔH is the activation energy, k is the Boltzmann constant, and T is absolute temperature. The activation energy can be expressed as

$$\Delta H = kT\ln\left(\frac{\dot{\varepsilon}_0}{\dot{\varepsilon}}\right) \quad \text{(Eq 6)}$$

where $\dot{\varepsilon}_0$ is a constant. In Eq. [6], the effect of temperature and strain rate is expressed in one term referred to as the rate parameter and will be discussed and used next. The flow stress (σ_f) can be written as an athermal component (σ_{ath}) and a thermal component (σ_{th}):

$$\sigma_f = \sigma_{ath} + \sigma_{th}. \quad \text{(Eq 7)}$$

The effect of strain rate and temperature is related to the thermal component and the athermal component may be taken as measured at quasi-static rate and a temperature high enough but without creep influence. High strain rate has similar effects on the thermal component to low temperature (Eq. 6). A rate parameter (Ref 27, 28) including the effect of both strain rate and temperature has been suggested, based on Eq. 6, in the form of $R = T\ln(\dot{\varepsilon}_o/\dot{\varepsilon})$. In this work, the athermal stress has been taken as the flow stress at 100 °C and 0.00075 s^{-1}, which is generally in agreement with Conrad's early work on Mg single crystals (Ref 29). For Mg, 100 °C is about 0.4 T/T_m; above this temperature, based on the deformation mechanism map, creep would have to be considered (Ref 30). Constitutive analysis was performed for ED samples because slip is the main deformation mechanism in these samples. The thermal yield strength data of ED samples have been calculated and plotted as a function of the rate parameter with $\dot{\varepsilon}_0 = 5.3 \times 10^7 s^{-1}$, as shown in Fig. 16 ($\dot{\varepsilon}_0$ has been chosen based on the constant used for steels adjusted in proportion to the relative volume diffusion coefficients). For ED samples, the tensile yield strength depends linearly on the rate parameter:

$$\sigma_{YS} = \sigma_{YS(T=373K)} + \left[194.9 - 0.0208T\ln\left(\frac{5.3 \times 10^7}{\dot{\varepsilon}}\right)\right] \quad \text{(Eq 8)}$$

where the unit for σ_{YS} is MPa, T is Kelvin and $\dot{\varepsilon}$ is s^{-1}. Equation [8] is based on tensile yield strength between 150 MPa and 291 MPa in the strain rate range between 0.00075 and 9 s^{-1}. This formula should not be extrapolated beyond this experimental range without further data.

The thermal activation volume (V*) values can be compared with the volumes predicted from the dislocation theory and the deformation mechanisms may be deduced. If the rate of plastic deformation is controlled by a single thermally activated dislocation mechanism, the activation volume V* may be evaluated experimentally using the following relation (Ref 27, 28),

$$V^* = 2kT\left(\frac{\partial \ln\dot{\varepsilon}}{\partial\sigma}\right)_T \quad \text{(Eq 9)}$$

assuming that the relation between tensile stress σ and shear stress τ is $\sigma = 2\tau$. This equation can be rewritten as

$$V^* = -2k\frac{d\left(T\ln\left(\frac{\dot{\varepsilon}_0}{\dot{\varepsilon}}\right)\right)}{d\sigma} \quad \text{(Eq 10)}$$

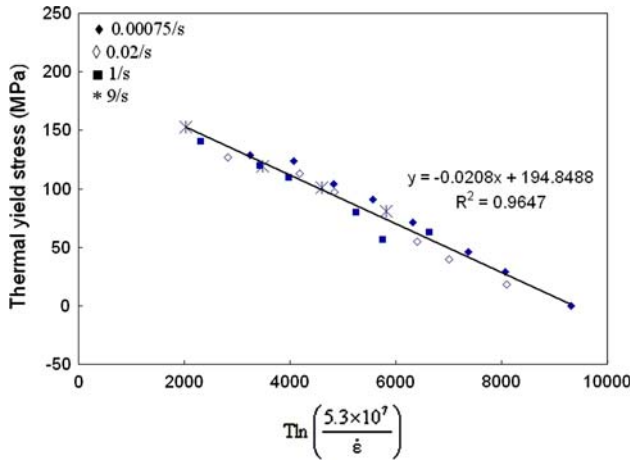

Fig. 16 Thermal yield stress as a function of strain rate and temperature of tensile ED samples

It follows that the linear relation of the stress versus rate parameter (Fig. 16) indicates a constant activation volume (38 $\mathbf{b}^3$ where $\mathbf{b}$ is the Burgers vector for magnesium). As summarized by Conrad (Ref 27, 28), a possible controlling mechanism for pure Mg could be intersection of dislocations; however, this corresponds with an activation volume $V^* = 10^2\text{-}10^3\ \mathbf{b}^3$, which is much larger than that observed in this work. The activation volumes $V^* = 10^1\text{-}10^2\ \mathbf{b}^3$ are in the range of those for overcoming the Peierls-Nabarro stress and/or cross slip, as summarized in (Ref 28). However, the activation volumes would be expected to increase with temperature for the Peierls-Nabarro stress and/or cross slip because the thermal stress decreases with temperature which should increase the activation distance (Ref 27, 28). However, the activation volume for AM30 extrusion was found to be constant. Since AM30 contains a large amount of solute atoms of Al and Mn (see Table 1), the solute atoms may have a significant influence on thermal activation in AM30. Therefore, the controlling deformation mechanism for the ED samples of AM30 alloy could also be dislocation interaction with solute atoms.

5. Summary

A magnesium alloy AM30 extrusion has been characterized to provide a database for constitutive analysis and crashworthiness simulation. The AM30 extrusion has a strong texture which has a profound effect on mechanical properties. Tensile deformation along the extrusion direction (ED) involved limited twinning, but tensile deformation along the TD showed significant twinning during the first 6-8% strain. Tensile stress-strain curves along ED can be roughly approximated by a power-law relation while those along the TD exhibited sigmoidal stress-strain curves.

Tensile tests performed along ED exhibited significant effects of strain rate and temperature on flow strength. The yield strengths of ED samples depend linearly on the rate parameter $T\ln(5.3 \times 10^7/\dot{\varepsilon})$ within the data obtained in this work, implying a constant activation volume. The effect of strain rate and temperature on TD samples is smaller than for ED samples during the initial stage of deformation, as expected from the larger amount of twinning activity (explained by the effect of texture).

Nominal strain energy densities up to 10% engineering strain and to fracture were calculated from engineering stress-strain curves. The specific tensile performance of Mg extrusions, taking into account yield strength, ductility and density, compares favorably to Al alloys and high-strength steels owing to their low densities and good ductility.

Acknowledgments

This work is part of the Canadian crashworthiness R&D task of an on-going international Magnesium Front-End Research and Development (MFERD) project. The MFERD project was first presented in the Canada-China-USA workshop on magnesium technologies, Dearborn, Michigan, Oct 17-19, 2005. The Project Steering Committee and Project Technical Committee (especially Drs. J. Lo, K. Sadayappan, A. A. Luo, and J. Jackman) set the objectives for the task and support for its success. US and China task leaders, D. Wagner and Z. Liu, are gratefully acknowledged for useful discussions and help. The work was funded by the Climate Change Technology and Innovation Initiative, Government of Canada. Large solid extrusions of AM30 alloy were provided by General Motors Research and Development Center, Warren, MI for which Dr. A.A. Luo is gratefully acknowledged for his help. Texture measurements of the as-received extrusions were performed in McGill University and we would like to acknowledge Prof. Jerzy Szpunar, Dr. Hualong Li, and Mr. Slawomir Poplawski for their assistance. We would like to thank Mr. Bob Eagleson for performing mechanical tests, Ms. Renata Zavadil and Ms. Pei Liu for metallographic and fractographic examinations, and Ms. Catherine Bibby for preparing TEM samples.

References

1. N.-Y. Li, R.J. Osborne, B.M. Cox, and D.E. Penrod, "Magnesium Engine Cradle—The USCAR Structural Cast Magnesium Development Project," SAE Technical Paper Series 2005-01-0337, 2005
2. Anon, Innovations in Materials Technology, *Adv. Mater. Process.*, 2006, **164**, p 9
3. A.A. Luo, E. Nyberg, K. Sadayappan, and W. Shi, "Magnesium Front End Research & Development—A Canada–China–USA Collaborative Project," presentation at *Magnesium Technology*, TMS 2007 Annual Meeting, Feb 25–Mar 1, 2007, Orlando, FL, USA
4. A.A. Luo and A.K. Sachdev, Magnesium Wrought Alloy Having Improved Extrudability and Formability, United States Patent 20050194072 (2005)
5. A.A. Luo and A.K. Sachdev, Development of a New Wrought Magnesium–Aluminum–Manganese Alloy AM30, *Metall. Mater. Trans. A*, 2007, **38**, p 1184–1192
6. L. Jiang, J.J. Jonas, A.A. Luo, and A.K. Sachdev, Twinning-Induced Softening in Polycrystalline AM30 Mg Alloy at Moderate Temperatures, *Scr. Mater.*, 2006, **54**, p 771–775
7. L. Jiang, J.J. Jonas, R.K. Mishrab, A.A. Luo, A.K. Sachdev, and S. Godet, Twinning and Texture Development in Two Mg Alloys Subjected to Loading Along Three Different Strain Paths, *Acta Mater.*, 2007, **55**, p 3899–3910
8. I.J. Polmear, *Light Alloys* (Second Edition), Edward Arnold, A Division of Hodder & Stoughton, London, 1989, p 200–210
9. K. Sato, A. Yoshitake, Y. Hosoya, and T. Yokoyama, A Study on Improving the Crashworthiness of Automotive Parts by Using Hat Square Columns, *Proceedings of International Body Engineering Conference,* IBEC(1997), Interior, Safety and Environment, vol. 30, 1997, p 89–97
10. B. Yan and K. Xu, High Strain Rate Behavior of Advanced High Strength Steels for Automotive Applications, *Conference Proceedings of the 44th Mechanical Working and Steel Processing*, vol. XL, ISS, 2002, p 493–509
11. S. Oliver, T.B. Jones, and G. Fourlaris, Dual Phase Versus TRIP Strip Steels: Comparison of Dynamic Properties for Automotive Crash Performance, *Mater. Sci. Technol.*, 2007, **23**, p 423–431
12. Sp.G. Pantelakis, N.D. Alexopoulos, and A.N. Chamos, Mechanical Performance Evaluation of Cast Magnesium Alloys for Automotive and Aeronautical Applications, *J. Eng. Mater. Technol.*, 2007, **129**, p 422–430
13. A.A. Luo, R.C. Kubic, and J.M. Tartaglia, Microstructure and Fatigue Properties of Hydroformed Aluminum Alloys 6063 and 5754, *Metall. Mater. Trans. A*, 2003, **34**, p 2549–2557
14. *ULSAB-AVC TTD#6* (Technology Transfer Dispatch #6) available from http://www.ULSAB-AVC.org or http://www.autosteel.org. Accessed August 2005
15. C.S. Roberts, *Magnesium and Its Alloys*, John Wiley & Sons, Inc., New York, 1960, p 84–88
16. Z. Keshavarrz and M.R. Barnett, EBSD Analysis of Deformation Modes in Mg–3Al–1Zn, *Scr. Mater.*, 2006, **55**, p 915–918
17. M.R. Barnett, Z. Keshavarz, A.G. Beer, and D. Atwell, Influence of Grain Size on the Compressive Deformation of Wrought Mg–3Al–1Zn, *Acta Metall.*, 2004, **52**, p 5093–5103
18. M.R. Barnett, A Taylor Model Based Description of the Proof Stress of Magnesium AZ31 During Hot Working, *Metall. Mater. Trans. A*, 2003, **34A**, p 1799–1806

19. J. Koike, T. Kobayashi, T. Mukai, H. Watanabe, M. Suzuki, K. Maruyama, and K. Higashi, The Activity of Non-Basal Slip Systems and Dynamic Recovery at Room Temperature in Fine-Grained AZ31B Magnesium Alloys, *Acta Mater.*, 2003, **51**, p 2055–2065
20. M.R. Barnett, Twinning and the Ductility of Magnesium Alloys: Part II. "Contraction" Twins, *Mater. Sci. Eng. A*, 2007, **464**, p 8–16
21. S.R. Agnew, Plastic Anisotropy of Magnesium Alloy AZ31B Sheet, *Magnesium Technology 2002*, H.I. Kaplan (Ed.), TMS, 2002, p 169–174
22. S.R. Agnew, C.N. Tomé, D.W. Brown, T.M. Holden, and S.C. Vogel, Study of Slip Mechanisms in a Magnesium Alloy by Neutron Diffraction and Modeling, *Scr. Mater.*, 2003, **48**, p 1003–1008
23. R.W. Hertzberg, *Deformation and Fracture Mechanics of Engineering Materials*, 2nd Edition, John Wiley & Sons, 1983, p 105–121
24. C.N. Tome, S.R. Agnew, W.R. Blumenthal, M.A.M. Bourke, D.W. Brown, G.C. Kaschner, and P. Rangaswamy, The Relation Between Texture, Twinning and Mechanical Properties in Hexagonal Aggregates, *Mater. Sci. Forum*, **408–412**, Part 1, 2002, p 263–268
25. D.W. Brown, S.R. Agnew, M.A.M. Bourke, T.M. Holden, S.C. Vogel, and C.N. Tome, Internal Strain and Texture Evolution During Deformation Twinning in Magnesium, *Mater. Sci. Eng. A*, 2005, **399**, p 1–12
26. G.R. Johnson and W.H. Cook, A Constitutive Model and Data for Metals Subject to Large Strains, High Strain Rates and High Temperatures, *Proceedings of the 7th International Symposium on Ballistics*, The Hague, The Netherlands, 1983, p 541–547
27. H. Conrad, Thermally Activated Deformation of Metals, *J. Metals*, 1964, p 582–588
28. H. Conrad, The Cryogenic Properties of Metals, *High-Strength Materials, Proceedings of the Second Berkeley International Materials Conference*, V.F. Zackay (Ed.), June 15–18, 1964, University of California, Berkeley, John Wiley & Sons, Inc., New York, p 436–509
29. H. Conrad, R. Armstrong, H. Wiedersich, and G. Schoeck, Thermally-Activated Glide in Magnesium Crystals from 4.2 to 420 K, *Phil. Mag.*, 1961, **VI**, p 177–188
30. H.J. Frost and M.F. Ashby, *Deformation-Mechanism Maps*, Pergamon Press, Oxford, UK, 1982, p 43–49